Article

Discovery Medicine 2024; 36(183): 739–752
https://doi.org/10.24976/Discov.Med.202436183.70

Investigating the Impact of First-Line Anti-Tuberculosis Drugs Encapsulated in a Eugenol-Based Nanoemulsion on Human Serum Albumin

Parvathy Mohan Menon[1], Natarajan Chandrasekaran[2,*], George Priya Doss C[1,*]

[1]Department of Integrative Biology, School of Bioscience and Technology, Vellore Institute of Technology, 632014 Vellore, India
[2]Centre for Nanobiotechnology, Vellore Institute of Technology, 632014 Vellore, India
*Correspondence: nchandrasekaran@vit.ac.in; nchandra@hotmail.com (Natarajan Chandrasekaran); georgepriyadoss@vit.ac.in (George Priya Doss C)
Published: 20 April 2024

Background: Eugenol exhibits broad-spectrum antibacterial and anti-inflammatory properties. However, cytotoxicity at high concentrations limits the full utilization of eugenol-based drug complexes. Formulations of multidrug-loaded eugenol-based nanoemulsions have reduced cytotoxicity; however, it remains crucial to understand how these eugenol complexes interact with primary human carrier proteins to design and develop therapeutic alternatives. Consequently, this study primarily aims to investigate the impact on Human Serum Albumin (HSA) when it interacts with eugenol-based complexes loaded with first-line anti-tuberculosis drugs.

Methods: This study used various spectroscopic such as UV-visible spectroscopy, Fluorescence spectroscopy, Fourier-transform infrared spectroscopy and computational methods such as molecular docking and 100 ns molecular simulation to understand the impact of eugenol-based first-line anti-tuberculosis drug-loaded nanoemulsions on HSA structure.

Results: The binding of the HSA protein and eugenol-based complexes was studied using UV-visible spectroscopic analysis. Minor changes in the fluorophores of the protein further confirmed binding upon interaction with the complexes. The Fourier-transform infrared spectra showed no significant changes in protein structure upon interaction with eugenol-based multidrug-loaded nanoemulsions, suggesting that this complex is safe for internal administration. Unlike eugenol or first-line anti-tuberculosis alone, molecular docking revealed the strength of the binding interactions between the complexes and the protein through hydrogen bonds. The docked complexes were subjected to a 100 ns molecular dynamics simulation, which strongly supported the conclusion that the structure and stability of the protein were not compromised by the interaction.

Conclusions: From the results we could comprehend that the eugenol (EUG)-drug complex showed greater stability in HSA protein structure when compared to HSA interacting with isoniazid (INH), rifampicin (RIF), pyrazinamide (PYR), or ethambutol (ETH) alone or with EUG alone. Thus, inferring the potential of EUG-based drug-loaded formulations for a safer and efficient therapeutic use.

Keywords: eugenol; first-line anti-TB drugs; HSA; nanoemulsions; spectroscopic technique; *in-silico* technique

Introduction

Essential oils extracted from aromatic plants, such as clove buds, cinnamon leaves, basil, and neem seeds, have long been known for their anti-inflammatory, antibacterial, and anti-stress properties [1]. These oils are volatile hydrophobic liquids that are typically light to rarely colored. Contrary to what their name suggests, they are not true oils but comprise various bioactive compounds, such as alkaloids, polyphenols, saponins, and terpenes [2]. Eugenol (EUG) is a bioactive compound that is a major component of *Syzygium aromaticum* (clove) and *Cinnamomum zeylanicum* (cinnamon, Sri Lankan origin). It is a secondary metabolite with a phenylpropanoid group found in aromatic plants (Fig. 1A) and is one of the most promising bioactive compounds extracted from natural sources [3,4]. EUG has been studied against a wide range of pathogenic microorganisms, such as *Salmonella typhi* [5,6], *Shigella flexneri* [7], *Escherichia coli* [8,9], Ebola virus [10], drug-resistant strains of *Klebsiella pneumoniae* [11], *Mycobacterium tuberculosis* [12,13], and severe acute respiratory syndrome coronavirus 2 [14].

Despite these benefits, the use of EUG as a treatment method is limited because of the potential cytotoxic effects of high concentrations of crude EUG extracts [15]. Several nano-based delivery systems have been developed to address this issue and improve drug administration in humans [16–18]. Among these systems, nanoemulsions have gained prominence because of the formation of monodisperse stable nanosized emulsion droplets that can deliver different hydrophobic pharmaceutically active components that are normally difficult to administer [19]. They are also non-toxic and exhibit improved bioavailability [20].

Copyright: © 2024 The Author(s). Published by Discovery Medicine. This is an open access article under the CC BY 4.0 license.
Note: *Discovery Medicine* stays neutral with regard to jurisdictional claims in published maps and institutional affiliations.

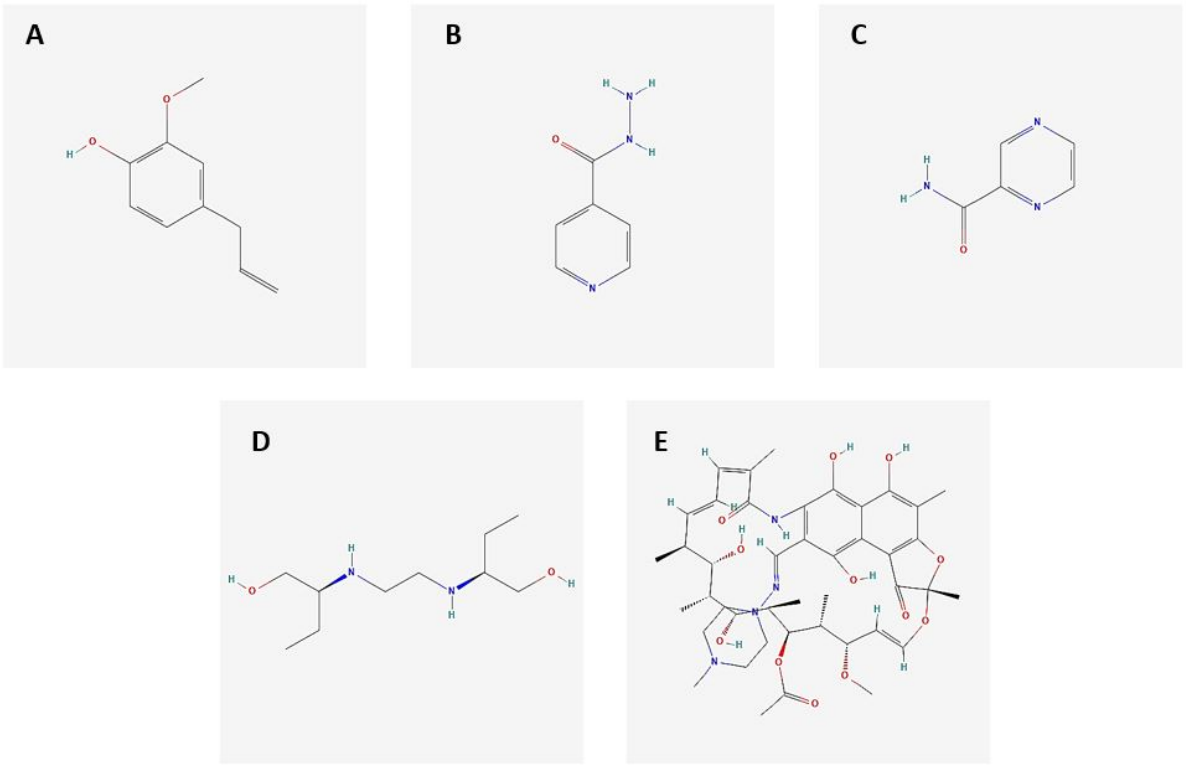

Fig. 1. Two-dimensional chemical structure depiction of ligands (A) eugenol, (B) isoniazid, (C) pyrazinamide, (D) ethambutol, and (E) rifampicin retrieved from PubChem.

Experimental studies have shown that EUG oil nanoformulations improve antibacterial activity against various bacterial strains [21–23]. Similarly, other studies have detailed various parameters demonstrating that the nanoformulations of essential oils containing eugenol is a much better alternative to crude EUG-based oils, due to enhanced antibacterial activity [24–26], improved photostability [27], and effective treatment of inflammation and periodontitis [28]. Hemaiswarya *et al*. [29] demonstrated the synergistic effects of eugenol and antibiotics against different gram-negative bacteria.

This has led to the development of EUG-based nanoemulsions loaded with multiple anti-tuberculosis (TB) drugs and the study of their efficacy against various *Mycobacterium tuberculosis* strains [30]. Given the potential of these drugs as alternative treatment methods, it is crucial to understand how they interact with various proteins in humans. Insights into drug stability and toxicity can be gained from the overall process of drug-protein interactions. Understanding the binding mechanisms of anti-TB drugs to proteins can significantly aid in designing drugs with improved efficacy and lower toxicity. To understand this, we must examine how these drugs interact with carrier proteins responsible for handling these molecules in the circulatory system. Plasma proteins in the human circulatory system include albumin, globulin, and fibrinogen [31]. Albumin is the most abundant protein, constituting approximately 60% of the total plasma protein content in the bloodstream. Despite the production of albumin proteins in the human liver, most of them are released into the bloodstream. When released into the bloodstream, they regulate oncotic pressure, thus maintaining blood flow [32]. They also function as transporters of exogenous and endogenous ligands. They are known to interact reversibly with various molecules, including hydrophobic drugs, thereby enhancing their solubility and making them crucial proteins for human studies [33].

Human Serum Albumin (HSA), a monomeric protein with a molecular weight of 66 kDa, is abundant in human plasma. It contains three homologous helical domains (I, II, and III), each of which is further divided into subdomains A and B [34]. Notably, subdomain A of domains II and III, known as Sudlow sites II, exhibits superior binding affinity for drugs and hormones and I. Although site II is less flexible and smaller than site I, it demonstrates a higher binding efficiency, particularly for hydrophobic interactions. Conversely, site I is primarily involved in hydrophobic interactions [35]. The intramolecular forces acting on the major fluorophores in the protein govern the binding of molecules to HSA. Because of these interactions, tryptophan, tyrosine, and phenylalanine are the three key residues monitored for alterations [36]. Any minor changes in these flu-

orophores can signify significant functional changes in the protein, potentially affecting the bioavailability and lifespan of drugs in the circulatory system. Interactions between different drug moieties and proteins can be studied using analytical and computational techniques [37]. UV-visible spectroscopy allows the examination of the binding nature of a compound with HSA under varying conditions, such as different concentrations. Fluorescence spectroscopy techniques can further elucidate changes in the structural stability of a protein upon interaction with compounds [38]. These findings have been corroborated by Fourier-transform infrared (FTIR) spectroscopy analysis, which has also been used to investigate conformational changes in the protein due to interactions [39]. *In-silico* studies, such as molecular docking and molecular simulations, have validated experimental data by providing information on the types of binding interactions and binding energies formed during protein-compound interactions [40–43]. Therefore, we combined these techniques to allow a comprehensive understanding of the conformational stability of HSA against multiple drug-loaded EUG-based nanoemulsions that were initially formulated for TB treatment.

This study aimed to investigate the interactions between HSA and EUG-based nanoemulsions loaded with multiple anti-TB drugs. Upon administration of HSA and eugenol-based nanoemulsions containing the drugs to humans, there may be some interactions that can cause structural changes in the HSA protein. We aimed to study these changes using various spectroscopic methods, including UV-visible spectroscopy, fluorescence spectroscopy, and FTIR spectroscopy. The findings were validated using molecular docking and simulation studies. We aimed to gain insights into how HSA is affected by a combination of eugenol and first-line anti-TB drugs. This may pave the way for alternative treatment methods for TB.

Materials and Methods

Analytical-grade chemicals, including HSA, rifampicin (RIF), ethambutol (ETH), pyrazinamide (PYR), and isoniazid (INH), were procured from HiMedia Laboratories (Mumbai, India). Additional reagents, such as eugenol oil, Tween 80, and phosphate buffer (pH 7.2) were obtained from Sigma-Aldrich (St Louis, MO, USA). All experiments were conducted using ultrapure water with a resistance of 18.3 Mcm^{-1}, condensed using a CascadaTM BIO-water purifier purchased from Pall India Pvt., Ltd. (Mumbai, India).

Formulation and Characterization of Drug-Loaded Nanoemulsions

A nanoemulsion loaded with multiple first-line antituberculosis drugs (RIF, INH, PYR, and ETH) was prepared using 4.5% eugenol oil, 22% Tween 80, and water. This preparation was prepared using an ultrasonicator (Vibra-Cell; Sonics & Materials, Inc, Newtown, CT, USA), operating for 8 min at an intensity of 40% and a temperature of 4 °C. The resulting drug-loaded nanoemulsion exhibited a mean droplet size of 37.7 nm, according to a previous report [30].

Spectroscopic Analyses

UV-Visible Spectroscopy

The UV absorbance was quantified using a Jenway 6850 UV-visible spectrophotometer (Antylia Scientific, UK), which offers a resolution of 0.1 nm. A stock solution was prepared by weighing 3.5 mg/mL HSA and dissolving it in a phosphate buffer solution, which served as the control. The absorbance of HSA was then measured within a spectral range of 250–350 nm [44]. Subsequently, the drug-loaded nanoemulsions were allowed to interact with the prepared HSA solution. The baseline was corrected for each spectrum to ensure accuracy.

Fluorescence Spectroscopy

Fluorescence spectra were recorded using a Jasco FP-6500 spectrofluorometer with measurements taken in a 10 mm quartz cuvette. Samples of varying concentrations were incubated with HSA in an orbital shaker for 2 min. The excitation and emission wavelengths were set at 350 and 410 nm, respectively [45]. For synchronous spectroscopy, the spectral parameters were adjusted to excitation and emission bandwidths of 2.5 and 5 nm, with 215 nm and 350 nm, respectively. The scan speed was configured to 500 nm/min, and the sensitivity was low [46].

Three-Dimensional Fluorescence Spectroscopy

The three-dimensional (3D) fluorescence spectra of HSA were examined using a Jasco FP-6500 spectrofluorometer. The excitation and emission wavelengths were set at 300–500 nm. Both HSA alone and HSA in an interaction with a nanoemulsion loaded with an EUG-based drug were placed in a 10 mm quartz cuvette and scanned at 60,000 nm/min. The data obtained are presented as contour plots constructed using Origin Pro, version 2023b (Origin Lab Corporation, Northampton, MA, USA).

Attenuated Total Reflectance-FTIR Spectroscopy

FTIR spectroscopy was performed using a Spectrum One spectrometer (Perkin Elmer, Waltham, MA, USA) with a resolution of 1 cm^{-1}. The spectra of both HSA alone and HSA interacting with the drug-loaded nanoemulsion were analyzed in the 4500 to 400 cm^{-1} range at ambient temperature.

Computational Analysis

Protein and Ligand Retrieval

The crystal structure of the protein (ID 1AO6) [34] at a resolution of 2.50 Å was obtained from the RCSB Protein Data Bank (https://www.rcsb.org/search) and was used as

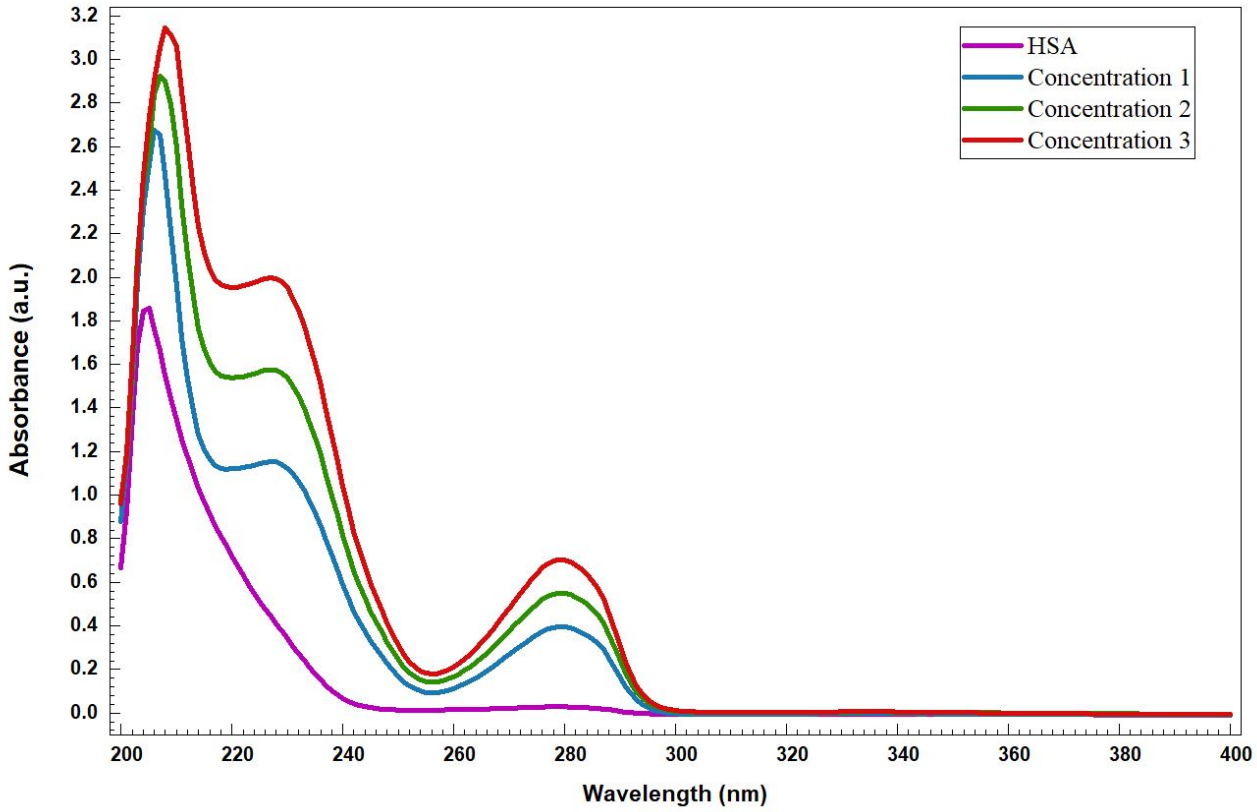

Fig. 2. UV-visible spectroscopy of human serum albumin interacting with different concentrations of drug-loaded eugenol nanoemulsions. The concentration of Human Serum Albumin (HSA) was kept constant at 1.2 mg/mL, and different drug-loaded eugenol nanoemulsions of 1.2 mg/mL (concentration-1), 1.6 mg/mL (concentration-2), and 2 mg/mL (concentration-3) were used.

the template for human HSA. Ligands were sourced from PubChem [47] (https://pubchem.ncbi.nlm.nih.gov/). The confirmed ligands included EUG (PubChem ID 3314), INH (PubChem ID 3767), PYR (PubChem ID 1046), RIF (PubChem ID 135398735), and ETH (PubChem ID 14052), as shown in Fig. 1. The active sites of protein 1AO6 were predicted using the web-based Computed Atlas of Surface Topography of Proteins (CASTp) tool [48] (http://sts.bioe.uic.edu/castp/index.html?4jii). The predicted binding sites, such as ARG257, ARG222, LYS199, HIS242, ARG218, and LYS195 [34], were further chosen for docking analysis as active sites for ligand binding. Similarly, the HOTSPOT wizard tool (http://loschmidt.chemi.muni.cz/hotspotwizard) [49] and a literature survey were used to identify the allosteric site for docking the EUG component.

Molecular Docking Studies

The HSA protein was docked with EUG at the allosteric site, and each drug component was individually docked at its respective active site using Auto Dock Software v4.2 (CA, USA) and Auto Dock Tools [50]. The protein structure for docking was initially prepared by removing the water molecules and adding polar hydrogen atoms. A 3D structure of standard size was generated near the binding sites. As part of the preparation of the protein structure, Gasteiger and Kollman charges and polar hydrogen bonds were added. This optimized protein was saved in PDBQT format for further docking [51]. Protein-ligand binding conformations were generated using the Lamarckian genetic algorithm. Five distinct docking conformations were performed, with the drugs docked in the targeted active sites and EUG docked in the allosteric site of the HSA protein. The protein-ligand complexes were visualized using BIOVIA Discovery Studio visualizer v20.1.0.19295, (Biovia, D.S. (2019) Discovery Studio Visualizer. San Diego, CA, USA) [52].

Molecular Dynamics Simulations

We performed molecular dynamics simulations using GROMACS version 2019.4 software (Stockholm, Sweden) with the CHARMM force field [53,54]. All physiological parameters, including hydrogen atoms, were maintained in a solvated box during the simulation. The system was hydrated using the TIP3 water model and neutralized with Na^+ and Cl^- ions [55]. The energized and equilibrated system was then subjected to a constant temperature and a constant pressure of 1 ps. Within the continuous flow of solvent, the protein-ligand complex was restricted until 100 ns all-atom simulations were accomplished. Nine simulations were executed, including HSA

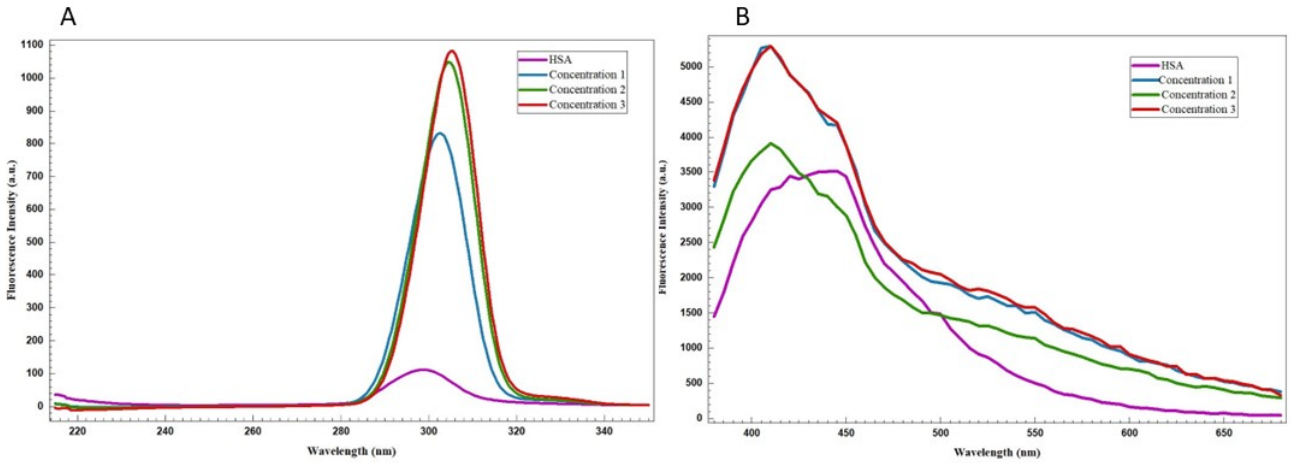

Fig. 3. Fluorescence spectroscopy of human serum albumin interacting with different concentrations of drug-loaded eugenol nanoemulsions. (A) Synchronous fluorescence spectroscopy. (B) Fluorescence emission spectra of HSA protein with different concentrations of drug-loaded eugenol nanoemulsions. The concentration of HSA was kept constant at 1.2 mg/mL, and different drug-loaded eugenol nanoemulsions of 1.2 mg/mL (concentration-1), 1.6 mg/mL (concentration-2), and 2 mg/mL (concentration-3) were used.

with EUG, HSA with each drug, and a combination of EUG and the individual drugs. Finally, vital molecular simulation trajectories such as root mean square deviation (RMSD), root mean square fluctuation (RMSF), the radius of gyration (Rg), the solvent-accessible surface area (SASA), and the number of hydrogen bonds, were calculated using GROMACS [56]. These were visualized using the QtGrace tool (https://www.x64bitdownload.com/downloads/t-64-bit-qtgrace-download-unmafskr.html) (Grace-5.1.22/QtGrace v0.2.6).

Binding Energy Calculations Using Molecular Mechanics-Poisson-Boltzmann Surface Area

The binding free energy of the protein and its interactions with various ligands were computed using the molecular mechanics-Poisson-Boltzmann surface area (MM-PBSA) method [57]. The calculation was performed using the g_mmpbsa package in the GROMACS software suite. The binding energies of HSA with the drugs and EUG compounds were estimated using the Poisson-Boltzmann equation:

$$\Delta G_{binding} = \Delta G_{complex} - (\Delta G_{ligand} + \Delta G_{protein}),$$

where $\Delta G_{binding}$ represents the binding free energy; $\Delta G_{complex}$ represents the complex free energy; and ΔG_{ligand} and $\Delta G_{protein}$ represent the free energy of the ligand and protein, respectively.

Results and Discussion

TB remains the leading cause of death due to infectious diseases globally. The challenges of drug resistance and cellular toxicity have complicated the discovery of novel treatment methods for TB. The interaction with HSA is a crucial step in the development of new therapeutic methods for humans. In this study, we investigated the binding of HSA to nanoemulsions loaded with EUG-based first-line anti-TB drugs using various spectroscopic and computational methods. The antimycobacterial inhibition properties of EUG and EUG-based essential oils were documented in our previous work. However, when considering these EUG-based nanoemulsion systems as a therapeutic method for human administration, their interaction with HSA is crucial. We examined the interactions of these drug-loaded EUG nanoemulsions with primary carrier proteins using UV-visible spectroscopy.

Spectroscopic Analysis

We examined the interactions between multiple anti-TB drugs loaded onto EUG-based nanoemulsions and HSA after internal administration in humans. We used UV-visible spectroscopy, a simple, yet effective, analytical technique, to investigate the structural changes in HSA. The protein exhibits a characteristic absorbance at approximately 280 nm due to the π-π^* transitions of the

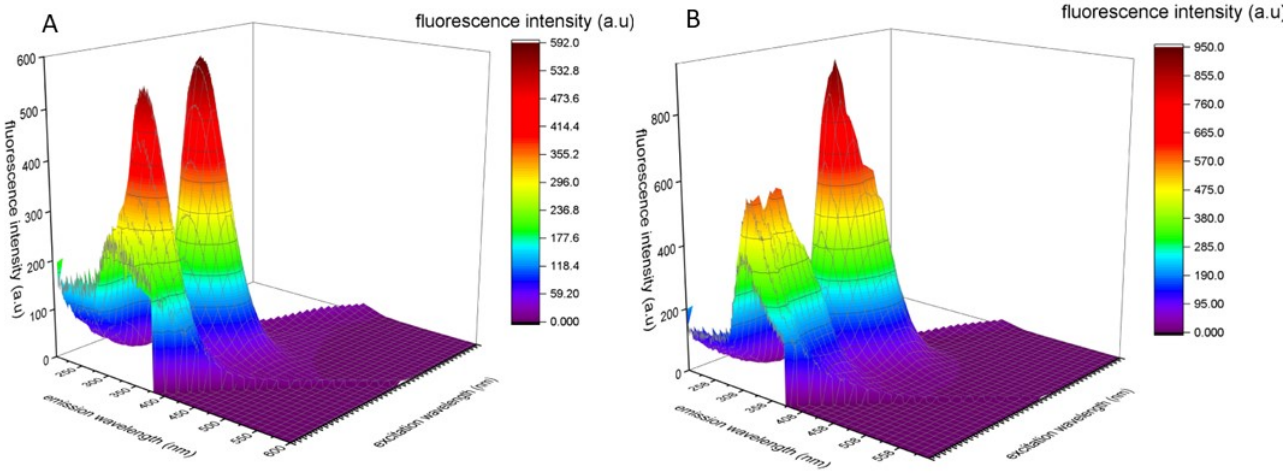

Fig. 4. Three-dimensional spectroscopy of HSA interacting with drug-loaded eugenol nanoemulsions. (A) 3D spectra of HSA before interacting with the drug-loaded nanoemulsions. (B) 3D spectra of HSA after interacting with the drug-loaded nanoemulsions.

tryptophan and tyrosine residue. This characteristic absorbance is shown in Fig. 2, the absorption peak intensity increased with increasing concentrations of the drug-loaded nanoemulsions, indicating an impact on the structural framework of the protein. The prominent tryptophan and tyrosine residue of HSA at 280 nm contributes to its fluorescence behaviour. As the UV-visible spectroscopy only a basic idea regarding the protein-ligand interaction, the synchronous fluorescence spectra shown in Fig. 3A revealed the difference of wavelength ($\Delta\lambda$) of 15 nm is characteristic of tyrosine, which showed an increase in intensity at 299.5 nm. This falls within the standard fluorescence emission wavelength range of HSA, spanning from 255 nm to 400 nm. Such behavior has been observed in previous study when HSA interacted with varying concentrations of drug-loaded nanoemulsions [58]. This change suggests conformational alterations within the protein upon interaction with the drug-loaded EUG nanoemulsions. While performing Intrinsic fluorescence studies (Fig. 3B) showed a a gradual increase in peak intensity between the range of 400 nm–450 nm which is again the characteristic wavelength range of HSA with increasing drug-loaded nanoemulsion concentrations.

3D fluorescence spectroscopy provided further insights into these conformational changes. Fig. 4 presents the 3D contour plots of the protein before and after interaction with the drug-loaded nanoemulsions, showing the maximum emission along with the excitation wavelength. There was no change in the emission spectra upon the addition of the drug-loaded nanoemulsions, but a reduction in intensity was observed. FTIR was conducted to study the structural and conformational dynamics of HSA in the presence and absence of drug-loaded nanoemulsions. Fig. 5 shows no significant changes except for the fingerprint area of EUG in both spectra. The amide bands, which are characteristic peaks of HSA and involved in its secondary structure, remained unchanged after interaction with the EUG-based multiple drug-loaded nanoemulsions, suggesting that secondary structures such as intermolecular β sheets, β sheets, and α helices within the protein were retained [59].

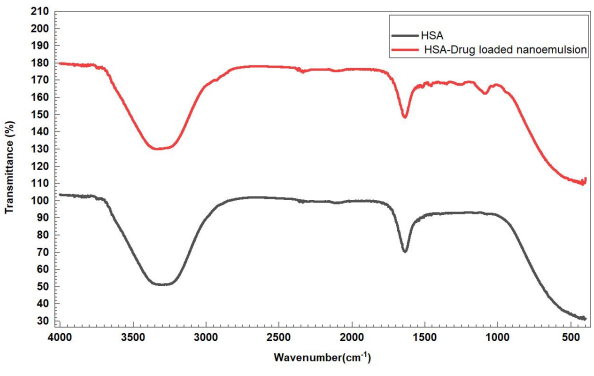

Fig. 5. Fourier-transform infrared spectra of HSA alone and with drug-loaded eugenol nanoemulsions.

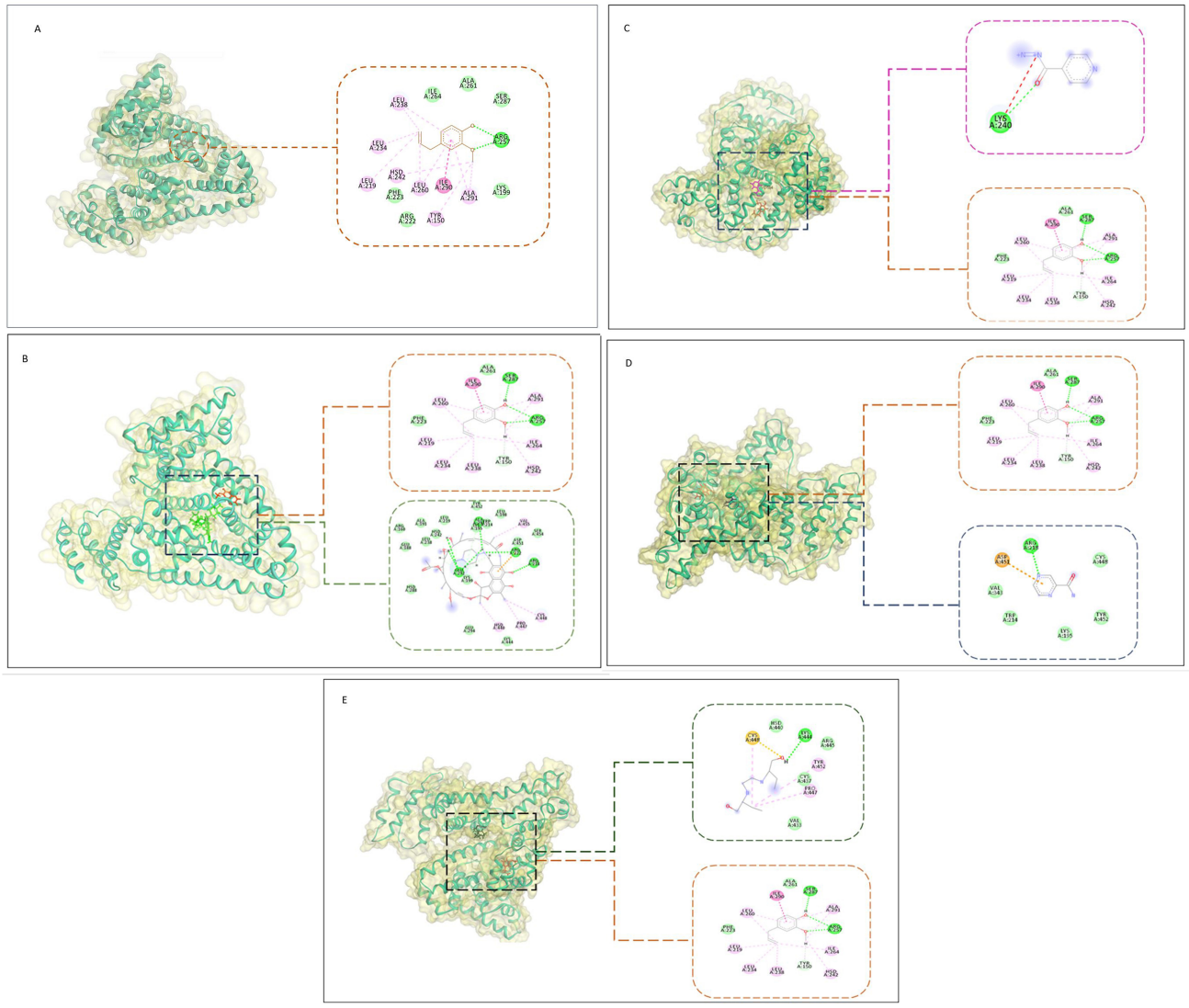

Fig. 6. Docking of HSA with different ligand combinations in 3D and 2D representations using BIOVIA Discovery Studio. Color representation is as follows: HSA protein is represented in a cyan blue solid ribbon; eugenol (EUG) is brown; and the drugs RIF, INH, PYR, and ETH are green, pink, blue, and black, respectively. The ligand interactions are focused within the black dotted box and 2D representations are shown for the (A) HSA-EUG complex (brown), (B) HSA-EUG-RIF complex (green), (C) HSA-EUG-INH (pink) complex, (D) HSA-EUG-PYR (blue) complex and (E) HSA-EUG-ETH (dark green) complex. RIF, rifampicin; ETH, ethambutol; PYR, pyrazinamide; INH, isoniazid.

Computational Analysis

In total, nine molecular docking experiments were conducted in triplicate. A 2D representation of protein-ligand binding is also provided along with the 3D structures, including the docking of HSA with EUG represented in Fig. 6A, and RIF, INH, PYR, and ETH alone, represented in **Supplementary Fig. 1A–D**). Finally, we docked the HSA protein with each complex, EUG-RIF, EUG-INH, EUG-PYR, and EUG-ETH, as shown in Fig. 6B–E. EUG was docked at the allosteric site of the protein, while the drugs were docked at the active site of the protein. Initially, HSA was docked with EUG alone with an average docking score of –6.9 kcal/mol with six conventional hydrogen bonds primarily at ARG257, as represented in Fig. 6A. Similarly, HSA was docked with individual drugs RIF, INH, PYR, and ETH with average binding energies of –7.8 kcal/mol, –4.7 kcal/mol, –3.8 kcal/mol, and –4.3 kcal/mol respectively. It was also observed that the protein formed 18, 11, 4, and 9 strong conventional hydrogen bonds with RIF, INH, PYR, and ETH, respectively (**Supplementary Fig. 1A–D**). Although we noticed a similar binding pattern with the drug-EUG complexes, they had higher binding energies and more hydrogen bonds. For instance, HSA bound with the EUG-RIF (Fig. 6B), EUG-INH (Fig. 6C), EUG-PYR (Fig. 6D), and EUG-ETH (Fig. 6E) complexes with an average binding energy of –7.9 kcal/mol with twenty conventional hydrogen bonds, mainly at ARG222, ARG218, GLU292, and ALA291; average binding energy of -8.1

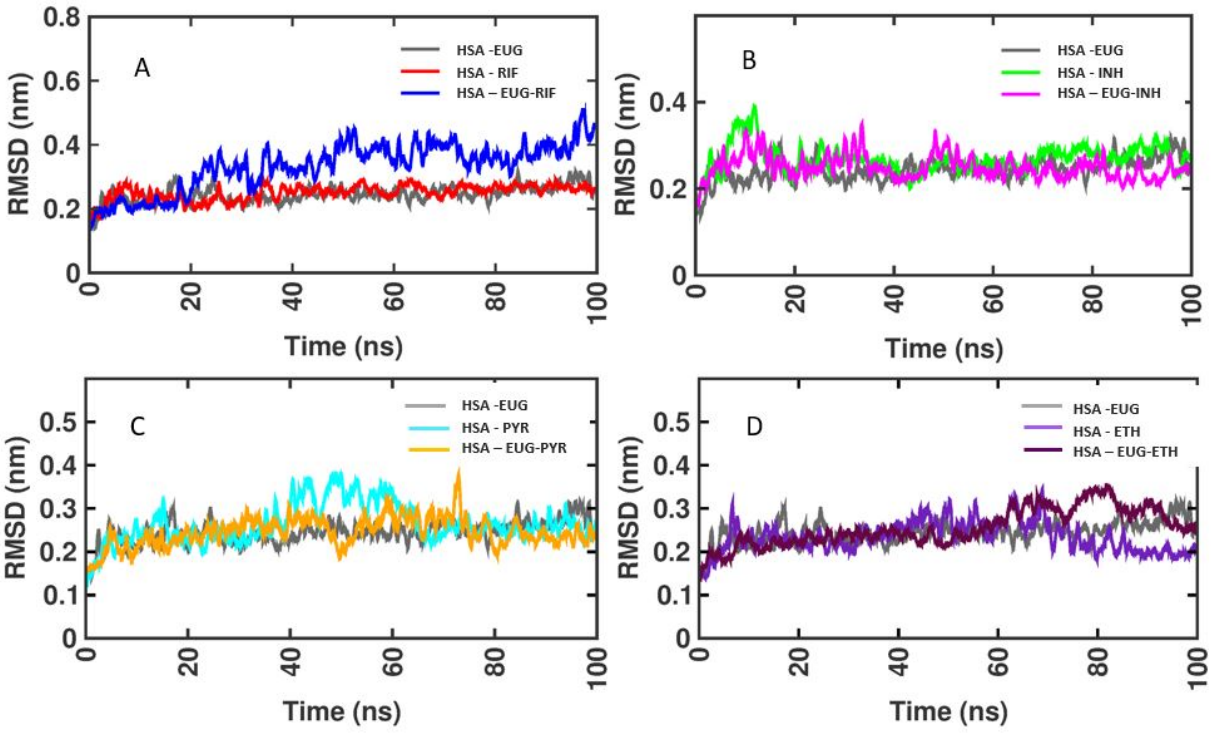

Fig. 7. Time evolution of root mean square deviation (RMSD) values for protein-drug complexes. (A) HSA-EUG (grey), HSA-RIF (red), and HSA-EUG-RIF (blue) complexes. (B) HSA-EUG (grey), HSA-INH (green), and HSA-EUG-INH (magenta) complexes. (C) HSA-EUG (grey), HSA-PYR (cyan), and HSA-EUG-PYR (yellow) complexes. (D) HSA-EUG (grey), HSA-ETH (lavender), and HSA-EUG-ETH (purple) complexes.

kcal/mol with 14 conventional bonds mainly at LYS240; average binding energy of –5.8 kcal/mol with 15 hydrogen bonds, mainly at ARG218; and average binding energy of –7.2 kcal/mol with eight hydrogen bonds in EUG-INH mainly at LYS444. We performed nine molecular simulations of 100 ns runs of the HSA-EUG, HSA-RIF, HSA-INH, HSA-PYR, HSA-ETH, HSA-EUG-RIF, HSA-EUG-INH, HSA-EUG-PYR, and HSA-EUG-ETH complexes.

Molecular dynamics simulations use various parameters such as RMSF, RMSD, Rg, SASA, and MMPBSA to predict changes in the structural stability of proteins [60–62]. The overall stability of the proteins was determined using RMSD plots. These plots show the degree of deviation in the protein structure when interacting with various ligands [63]. In the RMSD trajectories depicted in Fig. 7, a higher degree of structural deviation was observed when the protein interacted with different ligands. Fig. 7A shows that the protein structure deviated by an average of 0.018 nm when interacting with either RIF or EUG. However, an average of 0.239 nm deviation can be observed, when the protein interacts with EUG-RIF. This was not the case for other drugs, as they showed an average deviation of approximately 0.16 nm for the complexes with a single drug such as INH, PYR, ETH and approximately 0.15 nm for HSA-EUG-INH, HSA-EUG-PYR and HSA-EUG-ETH when compared to the structure of the protein when it interacted with EUG alone. However, because the RMSD plots showed deviations, we could not confirm the stability of the protein complexes. Further studies are needed to understand the flexibility of the protein, even when it interacts with ligands. This can be achieved by analyzing the RMSF values of the proteins. RMSF values are essentially the time averages of RMSD values, focusing on the computational adaptation of protein residues when interacting with different ligands over 100 ns in the simulation studies [64,65]. Protein stability appeared to improve when interacting with ligands indicated by the RMSD values. The RMSF values suggested no significant structural instability of the protein when it was combined with different ligands. The RMSF trajectories depicted in Fig. 8 generally exhibit an average fluctuation of less than 0.18 nm. This indicated that the complexes were flexible, with minor or no impact on the interaction of the EUG-drug complexes with HSA [66]. In addition to these parameters, the radius of gyration (Rg) analysis shown in Fig. 9, which indicates the compactness of protein complexes, showed variations in the Rg values, with an average of 0.02 nm over a 10,000 ps time interval. Notably, there was a sudden increase in the RMSD value after a time interval of 4000 ps when the protein interacted with the EUG-RIF complex. The solvent-accessible surface area (SASA) determines the number of free hydrophobic cores bound to solvent molecules. The

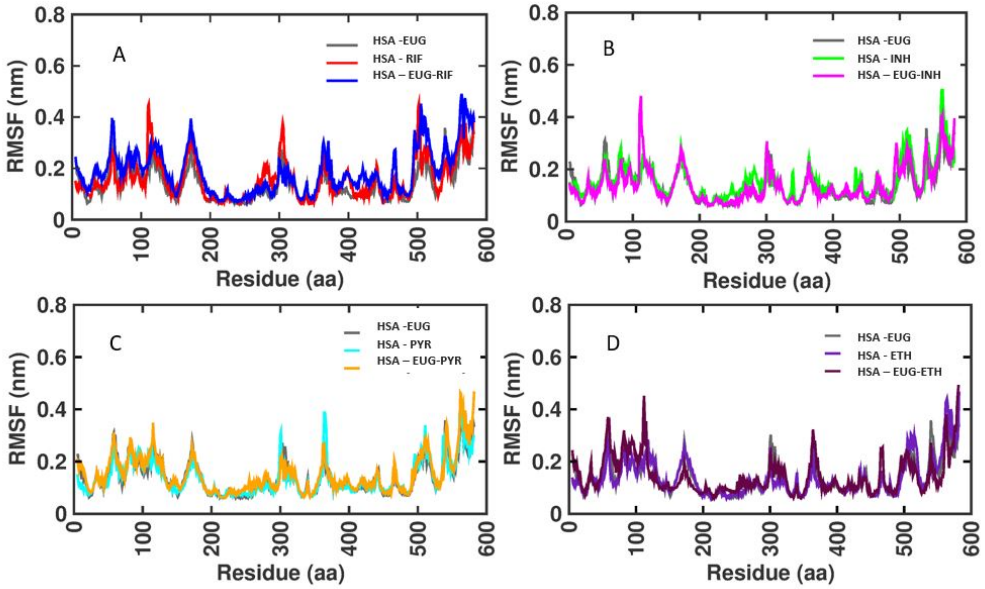

Fig. 8. Comparative RMSF values for the protein-drug complexes. (A) HSA-EUG (grey), HSA-RIF (red), and HSA-EUG-RIF (blue) complexes. (B) HSA-EUG (grey), HSA-INH (green), and HSA-EUG-INH (magenta) complexes. (C) HSA-EUG (grey), HSA-PYR (cyan), and HSA-EUG-PYR (yellow) complexes. (D) HSA-EUG (grey color), HSA-ETH (lavender color), and HSA-EUG-ETH (purple) complexes.

SASA trajectories depicted in Fig. 10 showed average areas of 302.6 nm^2, 297.2 nm^2, 297.9 nm^2, and 297.2 nm^2 available for solvent binding for the EUG-drug complexes, whereas the protein interacted with EUG alone without any drugs showed an area of 299.3 nm^2.

Determining the various binding affinities for each interaction provided significant insights into the stability of the protein-ligand complexes. To assess the strength of the interactions between the optimally docked ligands and HSA, the binding free energies of the docked complexes were determined using the MM-PBSA approach. The binding energies were broken down into their constituent energy components, namely, van der Waals energy, electrostatic energy, polar solvation energy, and SASA nonpolar solvation energy, to gain a deeper understanding of their individual contributions. From the MM-PBSA data, as tabulated in Table 1, we observed that the total binding energy was –56.727 +/– 13.191 kJ/mol, –80.634 +/– 31.014 kJ/mol, –15.908 +/– 11.705 kJ/mol, –13.631 +/– 49.763 kJ/mol, and –30.484 +/– 64.611 kJ/mol for HSA-RIF, HSA-INH, HSA-PYR, and has-ETH complexes, respectively. Similarly, we observed the total binding energies for HSA bound to EUG-INH, EUG-PYR, EUG-ETH, and EUG-PYR complexes to be –66.693 +/– 51.971 kJ/mol, –57.971 +/– 4.971 kJ/mol, –45.845 +/–1 0.250 kJ/mol, and –57.371 +/– 12.983 kJ/mol, respectively. Upon observing the binding sites, EUG and the drugs were found to be bound to the major active sites, as predicted in the initial crystal structure. This binding was sufficient to determine the significance of the HSA-EUG-drug complexes.

By applying computational techniques, such as docking, simulations, and MM-PBSA calculations, we determined that HSA exhibited a strong affinity for EUG and drug interactions. Furthermore, the combination of EUG with first-line anti-TB drugs demonstrated a higher affinity for HSA than that for the HSA-drug complexes. This was further validated by the increased number of hydrogen bonds observed in the docking analysis, indicating enhanced protein stability upon interaction, which was also reported by Patil *et al*., 2010 [67] and Sabour *et al*., 2022 [68]. On performing 100 ns molecular simulations using GROMACS and analyzing different parameters, such as RMSD values, we only found greater deviation for HSA-EUG and HSA-RIF complexes, which may be due to their larger hydrophobicity, which contributes to the stability of the protein [69]. When considered alongside the negative binding energies listed in Table 1, these data suggest a high degree of stability in the protein structure after interaction with the HSA-EUG-drug combination. However, the compactness of the protein structure did not appear to be compromised during the interaction of the HSA-EUG-drug complexes, as compared to the interactions with the HSA-drug or HSA-EUG. There was no evident change in the protein structure even after interacting with the ligand. By synthesizing these predictions, we can infer that the protein underwent certain structural alterations. However, these changes were insufficient to disrupt the role of a carrier protein. In summary, our study revealed the positive impact of EUG-based drug-loaded nanoemulsions on the structural stability of HSA when interacting with EUG-based drug-loaded na-

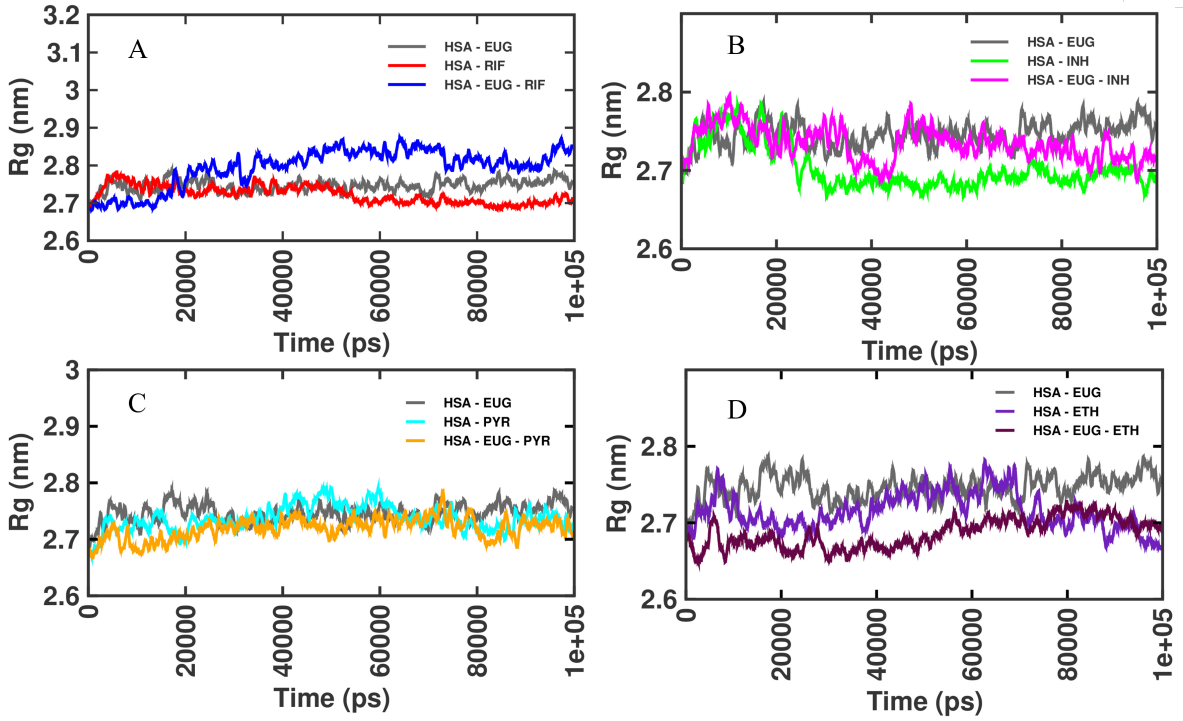

Fig. 9. Comparative radius of gyration (Rg) values for the complexes protein-drug complexes. (A) HSA-EUG (grey), HSA-RIF (red), and HSA-EUG-RIF (blue) complexes. (B) HSA-EUG (grey), HSA-INH (green), and HSA-EUG-INH (magenta) complexes. (C) HSA-EUG (grey), HSA-PYR (cyan), and HSA-EUG-PYR (yellow) complexes. (D) HSA-EUG (grey), HSA-ETH (lavender), and HSA-EUG-ETH (purple) complexes.

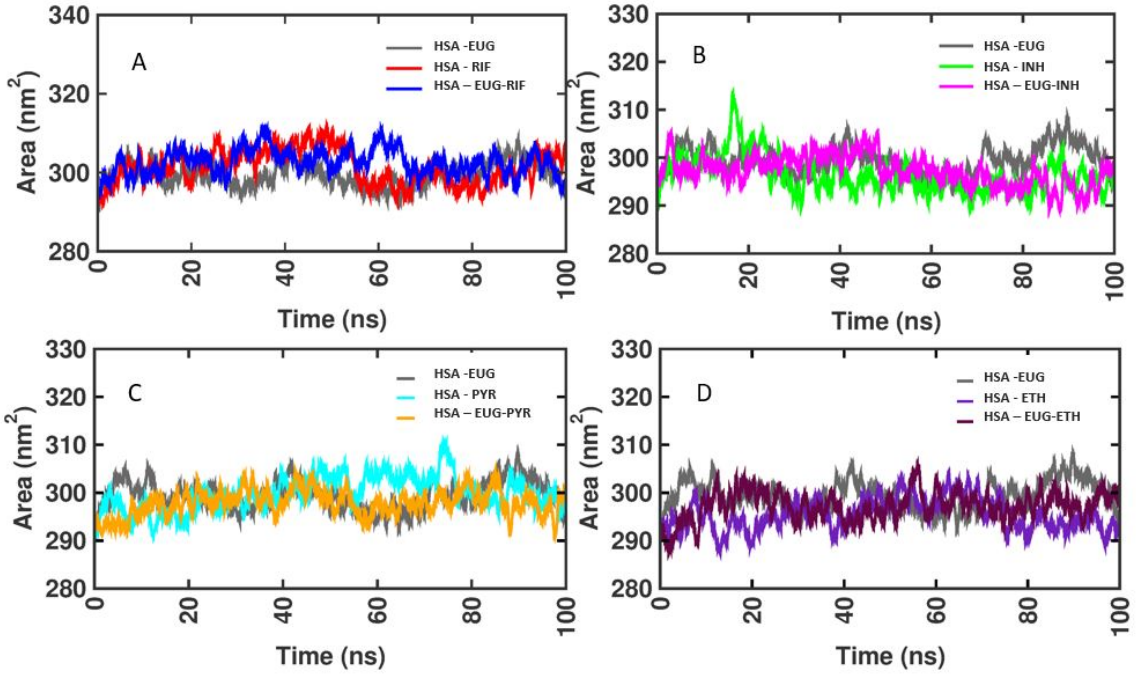

Fig. 10. Comparative solvent-accessible surface area (SASA) values for the protein-drug complexes. (A) HSA-EUG (grey), HSA-RIF (red), and HSA-EUG-RIF (blue) complexes. (B) HSA-EUG (grey), HSA-INH (green), and HSA-EUG-INH (magenta) complexes. (C) HSA-EUG (grey), HSA-PYR (cyan), and HSA-EUG-PYR (yellow) complexes. (D) HSA-EUG (grey), HSA-ETH (lavender), and HSA-EUG-ETH (purple) complexes.

Table 1. Summary of the binding free energy analysis using molecular mechanics-Poisson-Boltzmann surface area analysis of docked complexes.

Complexes	HSA-EUG	HSA-RIF	HSA-EUG- RIF	HSA-INH	HSA-EUG-INH	HSA-PYR	HSA-EUG-PYR	HSA-ETH	HSA-EUG-ETH
Energy	kJ/mol	kJ/mol	kJ/mol	kJ/mol	kJ/mol	kJ/mol	kJ/mol	kJ/mol	kJ/mol
van der Waal energy	–100.606 +/– 7.658	–231.262 +/– 18.307	– 45.420 +/– 41.563	– 47.164 +/– 33.217	– 10.290 +/– 12.299	–12.383 +/– 13.632	–3.694 +/– 7.554	–68.480 +/– 13.575	–100.894 +/– 4.363
Electrostatic energy	–8.436 +/– 9.452	–159.426 +/– 23.832	–17.554 +/– 21.342	–41.186 +/– 30.325	–1.086 +/– 7.111	–9.374 +/– 15.932	–1.272 +/– 1.661	–12.449 +/– 10.301	–6.649 +/– 7.273
Polar solvation energy	64.720 +/– 11.654	336.903 +/– 29.787	61.609 +/– 69.362	78.983 +/– 60.745	–6.868 +/– 33.732	10.441 +/– 56.806	35.311 +/– 67.310	44.696 +/– 13.138	62.073 +/– 13.827
SASA energy	–12.405 +/– 0.820	–26.849 +/– 1.392	–4.787 +/– 6.122	–6.533 +/– 4.585	–1.823 +/– 3.160	–2.315 +/– 2.037	0.140 +/– 1.712	–9.612 +/– 1.396	–12.300 +/– 0.422
Total Binding energy	–56.727 +/–13.191	–80.634 +/–31.014	–66.693 +/–51.971	–15.908 +/–11.705	–57.971 +/–4.971	13.631 +/–49.763	–30.484 +/–64.611	–45.845 +/–10.250	–57.371 +/–12.983

noemulsions. Notably, the EUG-drug complex exhibited greater stability than interactions with individual drugs or EUG alone. This enhancement suggests promising avenues for drug discovery. Hence, our results confirm the safety of EUG-based drug-loaded nanoemulsions for therapeutic purposes.

Conclusions

We investigated the interactions between EUG-based nanoemulsions loaded with first-line anti-TB drugs and HSA using analytical techniques. Our findings derived from spectroscopic and molecular modeling methods allowed us to elucidate the structure of human serum albumin and its interaction with EUG-based drug-loaded nanoemulsions. Importantly, we observed a positive outcome in terms of structural stability following this interaction. We observed that the EUG-drug complex showed greater stability in protein structure when interacting with HSA than when interacting with INH, RIF, PYR, or ETH alone or with EUG alone. Thus, it can be inferred that EUG enhances the structural stability of HSA and provides a promising approach for drug discovery. Based on these results, we conclude that our EUG-based drug-loaded nanoemulsions are safe for therapeutic use. Although our formulation is safe, its internalization mechanism must be validated via *in vitro* and *in vivo* experiments. The *in vitro* experiments included cell-based studies to understand the overall toxicity of the formulation when interacting with different cell lines. *In vivo* studies in different animal and infection models will provide an in-depth understanding of the mechanism of EUG-based drug-loaded nanoemulsions when administered internally. Our previous work [30] demonstrated its potency against drug-resistant strains of *Mycobacterium tuberculosis*. When dealing with such clinical challenges, we look forward to promising, budget-friendly, and convenient alternative therapies for treating patients with TB, including those with infections caused by multiple extensively drug-resistant strains.

Declaration of Generative AI in Scientific Writing

The authors declare that no AI tools were used to analyze and draw insights from data as part of the research process.

Availability of Data and Materials

The datasets used and/or analyzed during the current study are available from the corresponding authors upon reasonable request.

Author Contributions

NC has framed, supervised the execution, data interpretation, been involved in drafting the manuscript or revising it critically for important intellectual content, for spectroscopic analysis. GPDC has framed, supervised the execution, data interpretation, been involved in drafting the manuscript or revising it critically for important intellectual content data interpretation for the computational analysis. PMM has collected the data and performed the experimentation, analyzed it, and data interpretation, and been involved in drafting the manuscript or revising it critically for important intellectual content. PMM, NC, and GPDC have given final approval of the version to be published. All authors have participated sufficiently in the work to take public responsibility for appropriate portions of the content; and agreed to be accountable for all aspects of the work in ensuring that questions related to the accuracy or integrity of any part of the work are appropriately investigated and resolved.

Ethics Approval and Consent to Participate

Not applicable.

Acknowledgment

The authors express their gratitude to the Indian Council of Medical Research (ICMR) for providing the research grant that supported the project. The authors would like to take this opportunity to thank the management of Vellore Institute of Technology (VIT), Tamil Nadu, India for providing the necessary facilities to carry out this work.

Funding

This work was supported by the Indian Council of Medical Research (ICMR) for providing the research grant that supported the project entitled “Development of a high efficacy antibiotic-loaded in eugenol nanoemulsion as a nano delivery system against Multidrug-resistant tuberculosis (MDR-TB)” (file no. 5/8/5/48/Adhoc/2022/ECD-1).

Conflict of Interest

The authors declare no conflict of interest.

Supplementary Material

Supplementary material associated with this article can be found, in the online version, at https://doi.org/10.24976/Discov.Med.202436183.70.

References

[1] Bunse M, Daniels R, Gründemann C, Heilmann J, Kammerer DR, Keusgen M, *et al*. Essential Oils as Multicomponent Mixtures and Their Potential for Human Health and Well-Being. Frontiers in Pharmacology. 2022; 13: 956541.

[2] Sytar O, Smetanska I. Special Issue ”Bioactive Compounds from Natural Sources (2020, 2021)”. Molecules (Basel, Switzerland). 2022; 27: 1929.

[3] Nisar MF, Khadim M, Rafiq M, Chen J, Yang Y, Wan CC. Pharmacological Properties and Health Benefits of Eugenol: A Comprehensive Review. Oxidative Medicine and Cellular Longevity. 2021; 2021: 2497354.
[4] Fujisawa S, Murakami Y. Eugenol and Its Role in Chronic Diseases. Advances in Experimental Medicine and Biology. 2016; 929: 45–66.
[5] Hussain A, Brahmbhatt K, Priyani A, Ahmed M, Rizvi TA, Sharma C. Eugenol enhances the chemotherapeutic potential of gemcitabine and induces anticarcinogenic and anti-inflammatory activity in human cervical cancer cells. Cancer Biotherapy & Radiopharmaceuticals. 2011; 26: 519–527.
[6] Devi KP, Nisha SA, Sakthivel R, Pandian SK. Eugenol (an essential oil of clove) acts as an antibacterial agent against Salmonella typhi by disrupting the cellular membrane. Journal of Ethnopharmacology. 2010; 130: 107–115.
[7] Bai X, Li X, Liu X, Xing Z, Su R, Wang Y, *et al*. Antibacterial Effect of Eugenol on *Shigella flexneri* and Its Mechanism. Foods (Basel, Switzerland). 2022; 11: 2565.
[8] Olszewska MA, Gędas A, Simões M. The Effects of Eugenol, Trans-Cinnamaldehyde, Citronellol, and Terpineol on *Escherichia coli* Biofilm Control as Assessed by Culture-Dependent and -Independent Methods. Molecules (Basel, Switzerland). 2020; 25: 2641.
[9] Pei RS, Zhou F, Ji BP, Xu J. Evaluation of combined antibacterial effects of eugenol, cinnamaldehyde, thymol, and carvacrol against E. coli with an improved method. Journal of Food Science. 2009; 74: M379–M383.
[10] Lane T, Anantpadma M, Freundlich JS, Davey RA, Madrid PB, Ekins S. The Natural Product Eugenol Is an Inhibitor of the Ebola Virus *In Vitro*. Pharmaceutical Research. 2019; 36: 104.
[11] Liu W, Chen G, Dou K, Yi B, Wang D, Zhou Q, *et al*. Eugenol eliminates carbapenem-resistant *Klebsiella pneumoniae* via reactive oxygen species mechanism. Frontiers in Microbiology. 2023; 14: 1090787.
[12] de Almeida AL, Caleffi-Ferracioli KR, de L Scodro RB, Baldin VP, Montaholi DC, Spricigo LF, *et al*. Eugenol and derivatives activity against Mycobacterium tuberculosis, nontuberculous mycobacteria and other bacteria. Future Microbiology. 2019; 14: 331–344.
[13] Vidya Raj CK, Venugopal J, Muthaiah M, Chadha VK, Brammacharry U, Swappna M, *et al*. In-vitro anti-Mycobacterium tuberculosis effect of Eugenol. The Indian Journal of Tuberculosis. 2022; 69: 647–654.
[14] Naz F, Khan I, Baammi S, Islam A. Investigation of the interactions of HSA and SARS-CoV-2 papain-like protease against eugenol for novel COVID-19 drug discovery: spectroscopic and insilico study. Journal of Biomolecular Structure & Dynamics. 2023; 41: 10161–10170.
[15] Hartnoll G, Moore D, Douek D. Near fatal ingestion of oil of cloves. Archives of Disease in Childhood. 1993; 69: 392–393.
[16] Wilson RJ, Li Y, Yang G, Zhao CX. Nanoemulsions for drug delivery. Particuology. 2022. 64: 85–97.
[17] Patra JK, Das G, Fraceto LF, Campos EVR, Rodriguez-Torres MDP, Acosta-Torres LS, *et al*. Nano based drug delivery systems: recent developments and future prospects. Journal of Nanobiotechnology. 2018; 16: 71.
[18] Farokhzad OC, Langer R. Impact of nanotechnology on drug delivery. ACS Nano. 2009; 3: 16–20.
[19] Ma Y, Liu D, Wang D, Wang Y, Fu Q, Fallon JK, *et al*. Combinational delivery of hydrophobic and hydrophilic anticancer drugs in single nanoemulsions to treat MDR in cancer. Molecular Pharmaceutics. 2014; 11: 2623–2630.
[20] Samanta da Silva G, Maiara CV, Marianne KD, Fernanda RF, Priscila MC, Aline de OF, *et al*. Basil oil-nanoemulsions: Development, cytotoxicity and evaluation of antioxidant and antimicrobial potential. Journal of Drug Delivery Science and Technology. 2018; 46: 378–383.
[21] Fu X, Gao Y, Yan W, Zhang Z, Sarker S, Yin Y, *et al*. Preparation of eugenol nanoemulsions for antibacterial activities. RSC Advances. 2022; 12: 3180–3190.
[22] de Meneses AC, Sayer C, Puton BMS, Cansian RL, Araújo PHH, de Oliveira D. Production of clove oil nanoemulsion with rapid and enhanced antimicrobial activity against gram-positive and gram-negative bacteria. Journal of Food Process Engineering. 2019; 14: e13209.
[23] Kaur J, Mohamad T, Iqra R. Antimicrobial activity of bioactive compounds (thymoquinone and eugenol) and its nanoformulation therapeutic potential. Emerging modalities in mitigation of antimicrobial resistance (pp. 397–421). Springer International Publishing: Cham. 2022.
[24] Franklyne JS, Andrew Ebenazer L, Mukherjee A, Natarajan C. Cinnamon and clove oil nanoemulsions: novel therapeutic options against vancomycin intermediate susceptible Staphylococcus aureus. Applied Nanoscience. 2019; 9: 1405–1415.
[25] Ghosh V, Saranya S, Mukherjee A, Chandrasekaran N. Cinnamon oil nanoemulsion formulation by ultrasonic emulsification: investigation of its bactericidal activity. Journal of Nanoscience and Nanotechnology. 2013; 13: 114–122.
[26] Ghosh V, Mukherjee A, Chandrasekaran N. Eugenol-loaded antimicrobial nanoemulsion preserves fruit juice against, microbial spoilage. Colloids and Surfaces. B, Biointerfaces. 2014; 114: 392–397.
[27] Tiwari N, Ebenazer A, Franklyne JS, Sivakumar A, Mukherjee A, Chandrasekaran N. Drug loaded essential oil microemulsions enhance photostability and evaluation of in vitro efficacy. Photodiagnosis and Photodynamic Therapy. 2020; 29: 101638.
[28] Ahmad N, Ahmad FJ, Bedi S, Sharma S, Umar S, Ansari MA. A novel Nanoformulation Development of Eugenol and their treatment in inflammation and periodontitis. Saudi Pharmaceutical Journal: SPJ: the Official Publication of the Saudi Pharmaceutical Society. 2019; 27: 778–790.
[29] Hemaiswarya S, Doble M. Synergistic interaction of eugenol with antibiotics against Gram negative bacteria. Phytomedicine: International Journal of Phytotherapy and Phytopharmacology. 2009; 16: 997–1005.
[30] Menon PM, Chandrasekaran N, C GPD, Shanmugam S. Multidrug loaded eugenol-based nanoemulsions for enhanced antimycobacterial activity. RSC Medicinal Chemistry. 2023; 14: 433–443.
[31] Mathew J, Sankar P, Varacallo M. Physiology, Blood Plasma. In: StatPearls. StatPearls Publishing, Treasure Island (FL). 2023.
[32] Peters Jr T. All about albumin: biochemistry, genetics, and medical applications. Academic Press. 1995.
[33] Mishra V, Heath RJ. Structural and Biochemical Features of Human Serum Albumin Essential for Eukaryotic Cell Culture. International Journal of Molecular Sciences. 2021; 22: 8411.
[34] Sugio S, Kashima A, Mochizuki S, Noda M, Kobayashi K. Crystal structure of human serum albumin at 2.5 A resolution. Protein Engineering. 1999; 12: 439–446.
[35] Trynda-Lemiesz L. Paclitaxel-HSA interaction. Binding sites on HSA molecule. Bioorganic & Medicinal Chemistry. 2004; 12: 3269–3275.
[36] Sułkowska A. Interaction of drugs with bovine and human serum albumin. Journal of Molecular Structure. 2002: 614: 227–232.
[37] Yamasaki K, Chuang VTG, Maruyama T, Otagiri M. Albumin-drug interaction and its clinical implication. Biochimica et Biophysica Acta. 2013; 1830: 5435–5443.
[38] Ge F, Chen C, Liu D, Han B, Xiong X, Zhao S. Study on the interaction between theasinesin and human serum albumin by fluorescence spectroscopy. Journal of Luminescence. 2010; 130: 168–173.
[39] Filiz K, Erdogan DA, Özalp-Yaman S. Interaction of a novel platinum drug with bovine serum albumin: FTIR and UV-Vis

spectroscopy analysis. New Journal of Chemistry. 2015; 39: 5676–5685.

[40] Xu L, Hu YX, Li YC, Liu YF, Zhang L, Ai HX, *et al*. Study on the interaction of paeoniflorin with human serum albumin (HSA) by spectroscopic and molecular docking techniques. Chemistry Central Journal. 2017; 11: 116.

[41] Alhumaydhi FA, Aljasir MA, Aljohani ASM, Alsagaby SA, Alwashmi ASS, Shahwan M, *et al*. Probing the interaction of memantine, an important Alzheimer's drug, with human serum albumin: In silico and in vitro approach. Journal of Molecular Liquids. 2021; 340: 116888.

[42] Naveenraj S, Solomon RV, Mangalaraja RV, Venuvanalingam P, Asiri AM, Anandan S. A multispectroscopic and molecular docking investigation of the binding interaction between serum albumins and acid orange dye. Spectrochimica Acta. Part A, Molecular and Biomolecular Spectroscopy. 2018; 192: 34–40.

[43] Ranjan S, Dasgupta N, Sudandiradoss C, Ramalingam C, Kumar A. Titanium dioxide nanoparticle-protein interaction explained by docking approach. International Journal of Nanomedicine. 2018; 13: 47–50.

[44] Sugumar S, Nirmala J, Ghosh V, Anjali H, Mukherjee A, Chandrasekaran N. Bio-based nanoemulsion formulation, characterization and antibacterial activity against food-borne pathogens. Journal of Basic Microbiology. 2013; 53: 677–685.

[45] McClements DJ, Li Y. Structured emulsion-based delivery systems: controlling the digestion and release of lipophilic food components. Advances in Colloid and Interface Science. 2010; 159: 213–228.

[46] Eggers DK, Valentine JS. Molecular confinement influences protein structure and enhances thermal protein stability. Protein Science: a Publication of the Protein Society. 2001; 10: 250–261.

[47] Kim S, Chen J, Cheng T, Gindulyte A, He J, He S, *et al*. PubChem 2023 update. Nucleic Acids Research. 2023; 51: D1373–D1380.

[48] Tian W, Chen C, Lei X, Zhao J, Liang J. CASTp 3.0: computed atlas of surface topography of proteins. Nucleic Acids Research. 2018; 46: W363–W367.

[49] Bendl J, Stourac J, Sebestova E, Vavra O, Musil M, Brezovsky J, *et al*. HotSpot Wizard 2.0: automated design of site-specific mutations and smart libraries in protein engineering. Nucleic Acids Research. 2016; 44: W479–W487.

[50] Morris GM, Goodsell DS, Halliday RS, Huey R, Hart WE, Belew RK, *et al*. Automated docking using a Lamarckian genetic algorithm and an empirical binding free energy function. Journal of Computational Chemistry. 1998; 19: 1639–1662.

[51] Trott O, Olson AJ. AutoDock Vina: improving the speed and accuracy of docking with a new scoring function, efficient optimization, and multithreading. Journal of Computational Chemistry. 2010; 31: 455–461.

[52] BIOVIA. Dassault Systèmes. Discovery Studio Visualizer, v21.1.0.20298; Dassault Systèmes: San Diego, CA, USA. 2021. Available at: https://discover.3ds.com/discovery-studio-visualizer-download (Accessed: 21 December 2021).

[53] Van Der Spoel D, Lindahl E, Hess B, Groenhof G, Mark AE, Berendsen HJC. GROMACS: fast, flexible, and free. Journal of Computational Chemistry. 2005; 26: 1701–1718.

[54] Croitoru A, Park SJ, Kumar A, Lee J, Im W, MacKerell AD, Jr, *et al*. Additive CHARMM36 Force Field for Nonstandard Amino Acids. Journal of Chemical Theory and Computation. 2021; 17: 3554–3570.

[55] Hess B, Kutzner C, van der Spoel D, Lindahl E. GROMACS 4: Algorithms for Highly Efficient, Load-Balanced, and Scalable Molecular Simulation. Journal of Chemical Theory and Computation. 2008; 4: 435–447.

[56] Lindahl E, Abraham MJ, Berk H, Van Der Spoel D. GROMACS 2019.4 manual. GROMACS Doc. 2019.

[57] Kumari R, Kumar R, Open Source Drug Discovery Consortium, Lynn A. g_mmpbsa–a GROMACS tool for high-throughput MM-PBSA calculations. Journal of Chemical Information and Modeling. 2014; 54: 1951–1962.

[58] Zargar S, Wani TA, Alsaif NA, Khayyat AIA. A Comprehensive Investigation of Interactions between Antipsychotic Drug Quetiapine and Human Serum Albumin Using Multi-Spectroscopic, Biochemical, and Molecular Modeling Approaches. Molecules (Basel, Switzerland). 2022; 27: 2589.

[59] Usoltsev D, Sitnikova V, Kajava A, Uspenskaya M. Systematic FTIR Spectroscopy Study of the Secondary Structure Changes in Human Serum Albumin under Various Denaturation Conditions. Biomolecules. 2019; 9: 359.

[60] Chaieb K, Kouidhi B, Hosawi SB, Baothman OAS, Zamzami MA, Altayeb HN. Computational screening of natural compounds as putative quorum sensing inhibitors targeting drug resistance bacteria: Molecular docking and molecular dynamics simulations. Computers in Biology and Medicine. 2022; 145: 105517.

[61] Ahmad S, Navid A, Akhtar AS, Azam SS, Wadood A, Pérez-Sánchez H. Subtractive Genomics, Molecular Docking and Molecular Dynamics Simulation Revealed LpxC as a Potential Drug Target Against Multi-Drug Resistant Klebsiella pneumoniae. Interdisciplinary Sciences, Computational Life Sciences. 2019; 11: 508–526.

[62] Gurung AB, Ali MA, Lee J, Farah MA, Al-Anazi KM, Sami H. Molecular modelling studies unveil potential binding sites on human serum albumin for selected experimental and *in silico* COVID-19 drug candidate molecules. Saudi Journal of Biological Sciences. 2022; 29: 53–64.

[63] Pitaloka DAE, Ramadhan DSF, Arfan, Chaidir L, Fakih TM. Docking-Based Virtual Screening and Molecular Dynamics Simulations of Quercetin Analogs as Enoyl-Acyl Carrier Protein Reductase (InhA) Inhibitors of Mycobacterium tuberculosis. Scientia Pharmaceutica. 2021; 89: 20.

[64] Li MH, Luo Q, Xue XG, Li ZS. Molecular dynamics studies of the 3D structure and planar ligand binding of a quadruplex dimer. Journal of Molecular Modeling. 2011; 17: 515–526.

[65] Saeed M, Ashraf A, Sabir B, Zafar MO, Rashid MS. *In-silico* Screening of Origanum vulgare Phytocompounds as Potential Drug Agents Against Vp35 Protein of the Ebola Virus. bioRxiv. 2023. (preprint)

[66] Madeddu F, Di Martino J, Pieroni M, Del Buono D, Bottoni P, Botta L, *et al*. Molecular Docking and Dynamics Simulation Revealed the Potential Inhibitory Activity of New Drugs against Human Topoisomerase I Receptor. International Journal of Molecular Sciences. 2022; 23: 14652.

[67] Patil R, Das S, Stanley A, Yadav L, Sudhakar A, Varma AK. Optimized hydrophobic interactions and hydrogen bonding at the target-ligand interface leads the pathways of drug-designing. PloS One. 2010; 5: e12029.

[68] Sabour AA, Khan A, Alhuzani MR. Insight into the Interaction Mechanism of HSA with Aztreonam: A Multispectroscopic and Computational Approach. Molecules (Basel, Switzerland). 2022; 27: 7858.

[69] Pieroni M, Madeddu F, Di Martino J, Arcieri M, Parisi V, Bottoni P, *et al*. MD-Ligand-Receptor: A High-Performance Computing Tool for Characterizing Ligand-Receptor Binding Interactions in Molecular Dynamics Trajectories. International Journal of Molecular Sciences. 2023; 24: 11671.